RSC Publishing Faraday Discussions

ROY Revisited, Again: The Eighth Solved Structure

Journal:	*Faraday Discussions*
Manuscript ID	FD-ART-02-2018-000039.R2
Article Type:	Paper
Date Submitted by the Author:	24-Apr-2018

Complete List of Authors:	Tan, Melissa; New York University, Chemistry Shtukenberg, Alexander; New York University, Department of Chemistry Zhu, Shengcai; University of Nevada, Las Vegas, physical and astronomy Xu, Wenqian; Argonne National Laboratory, X-ray Science Division Dooryhee, Eric; Brookhaven National Laboratory, Nichols, Shane; New York University, Department Chemistry and Molecular Design Institute Ward, Michael; New York University, Chemistry Kahr, Bart; New York University Institute of Fine Arts, Chemistry Zhu, Qiang; University of Nevada Las Vegas, Physics and Astronomy

Journal Name

ARTICLE TYPE

Cite this: DOI: 10.1039/xxxxxxxxxx

ROY Revisited, Again: The Eighth Solved Structure†

Melissa Tan,[a] Alexander G. Shtukenberg,[a] Shengcai Zhu,[b] Wenqian Xu,[c] Eric Dooryhee,[d] Shane M. Nichols,[a,e] Michael D. Ward,[a] Bart Kahr,[a,f] and Qiang Zhu[b*]

Received Date
Accepted Date

DOI: 10.1039/xxxxxxxxxx

www.rsc.org/journalname

X-ray powder diffraction and crystal structure prediction (CSP) algorithms were used in synergy to establish the crystal structure of the eighth polymorph of 5-methyl-2-[(2-nitrophenyl)amino]-3-thiophenecarbonitrile (ROY), form R05. R05 crystallizes in the monoclinic space group $P2_1$ with lattice parameters a = 11.479(4) Å, b = 11.030(1) Å, c = 10.840(6) Å, β = 118.23(1)°. This is both the first acentric ROY polymorph, and the first with $Z' > 1$. The torsion angles defined by the S-C-N-C atom sequence of each molecule in the asymmetric unit (R05-1 and R05-2) are 44.9° and -34.0°. These values are between those previously determined for the red and orange forms of ROY. The crystal packing and intermolecular interactions in R05 are explained herein through Hirshfeld surface analysis and an updated energy stability ranking is determined using computational methods. Although the application of CSP was critical to the structure solution of R05, energy stability rankings determined using a series of DFT van der Waals (vdW)-inclusive models substantially differ from experiment, indicating that ROY polymorphism continues to be a challenge for CSP.

1 Introduction

There are ten polymorphs of 5-methyl-2-[(2-nitrophenyl)amino]-3-thiophenecarbonitrile, known simply as 'ROY' for its red, orange, and yellow crystals (Fig. 1). The abundance of colors exhibited by ROY, the peacock of molecular crystals, primarily arises from the conformational flexibility exhibited in the torsion angle, θ_{thio} (Fig. 1). Of the ten known polymorphs, the crystal structures of seven have been solved,[1,2] leaving three (Y04, RPL, and R05) unknown. Here, we report the crystal structure of one of these three, R05, an abbreviation for "red 2005", the most recently discovered ROY polymorph.[3]

For those who like to keep score, ROY once held the record as the organic compound with the most associated polymorphic structures: seven in total (solvates naturally excluded).[4] In 2013, flufenamic acid[5] surpassed ROY with eight crystal structures solved. More recently still, aripiprazole,[6] the anti-depressant sold as Abilify, joined the club of eight. By determining the structure of R05, ROY - a perennial favorite of fans of polymorphs, and a well-spring for theorists - again returns to the lead, albeit a three-way tie.

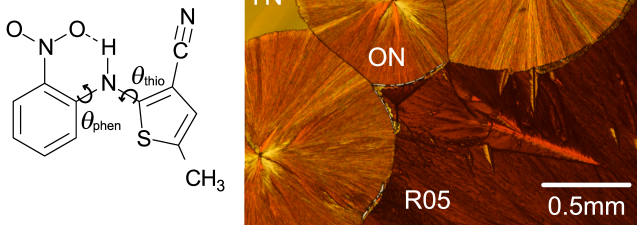

Fig. 1 ROY molecule (*left*). The torsion angles are indicated by θ_{thio} and θ_{phen}. Optical micrograph of spherulites of three ROY phases (YN, ON, R05) grown from the melt viewed with polarized light microscope (*right*).

R05 is distinguished from other ROY polymorphs for crystallizing in the enantiomorphous space group $P2_1$, and for having $Z' = 2$. These two independent molecules have different conformations, and to the extent that the photophysical properties of ROY can be approximated to the first order from molecular conformation, we observed from visible absorption spectra that R05 is more optically dense than any other polymorph of ROY that can

[a] *Department of Chemistry and Molecular Design Institute, New York University, 100 Washington Square East, Room 1001, New York City, NY, 10003, USA*
[b] *Department of Physics and Astronomy, High Pressure Science and Engineering Center, University of Nevada Las Vegas, Nevada, 89154, USA*
[c] *X-ray Science Division, Advanced Photon Source, Argonne National Laboratory, Argonne, Illinois, 60439, USA*
[d] *Photon Sciences Division, National Synchrotron Light Source II, Brookhaven National Laboratory, Upton, NY, 11973, USA*
[e] Department of Chemistry and Chemical Biology, Harvard University, 12 Oxford St, Cambridge, MA, 02138, USA
[f] *Department of Advanced Science and Engineering, Waseda University, 162-0056, Toykyo, Japan*
† Electronic Supplementary Information (ESI) available: [details of any supplementary information available should be included here]. See DOI: 10.1039/b000000x/

be grown from the melt.

2 Crystal Structure Determination

2.1 Crystallization

Thin films of ROY (< 5 μm) were prepared by melting 3-5 mg of powder ($C_{12}H_9N_3O_2S$, TCI, >97%, mp = 97.4 - 114.8° C) between a glass slide and coverslip on a hot plate. Spontaneous crystallization of the melt at room temperature yielded seven of the ten known polymorphs: Y, YN, YT04, Y04, ON, R, and R05. Except for YT04 and Y04, each of these forms appears distinct and can easily be identified with a polarizing light microscope. R05 grows as a smooth spherulite composed of fine, red-orange needles (Fig. 1) that transform to forms Y or R by movement of the growth front. If the metastable form R05 is in contact with other polymorphs of ROY, conversion can be complete in several hours. If, however, R05 is isolated, the conversion process occurs at a slower rate unfolding over the course of several weeks.

2.2 X-ray Powder Diffraction

The presence of R05 was confirmed by Raman spectroscopy (ω_{CN} = 2217 cm^{-1}, ω_{NH} = 3276 cm^{-1}) and powder X-ray diffraction. Measurements were collected at New York University of an as-grown spherulite using a Bruker AXS D8 Discover GADDS microdiffractometer (CuKα radiation, λ = 1.54178 Å) equipped with a VÅNTEC two-dimensional detector in reflection mode. This experiment corroborated previously published data indicating characteristic Bragg peaks at 2θ = 12.44, 12.47, 17.66, 18.38, 18.70, 23.13, 24.76, 26.44, 29.32, 31.22, and 33.19°.[3]

In order to achieve higher angular resolution necessary for indexing and structure solution, additional experiments were conducted at synchrotron sources. Initially, the data were collected at the 28-ID-2 (XPD) beamline at the National Synchrotron Light Source (NSLS-II), Brookhaven National Laboratory (BNL). Thin films of ROY were prepared from the melt at NYU and screened for R05. Immediately prior to data collection, crystallites of R05 were extracted with a scalpel, yielding < 1 mg of sample. The exterior wall of a 0.5 mm Kapton capillary was coated with a thin layer of Dow high vacuum grease (a silicone lubricant) and the sample was transferred onto the capillary by rolling the capillary through the powder. The measurement was performed at 250 K and λ = 0.18342 Åwith the sample to detector distance set at 1200 mm. The measured 2D pattern displays almost no preferential orientation of crystallites (Fig. 2). Unfortunately, because of the very short operational wavelength employed at BNL, the angular resolution was insufficient to index the cell.

A subsequent experiment with the same sample was performed one month later on the 17-BM beamline at the Advanced Photon Source (APS), Argonne National Laboratory. In the interim, the capillary was stored upright in a sealed container at 4°C. The sample was inspected at APS to determine whether conversion had begun. Although the major phase remained as form R05, a minor population of yellow crystallites had begun to grow, indicating the presence of at least one other polymorph. Two 30 second exposures were collected at 295 K (λ = 0.45336 Å, sample to detector distance = 800 mm). Both datasets were subsequently combined to create a single output file. The 2D pattern of these measurements displays evidence consistent with contamination from other phases in the form of dots and short arcs at 2θ positions that do not correspond to R05.[3] In addition, the APS pattern exhibits some preferential orientation of R05 crystallites, biasing the intensities of certain reflections (Fig. 2).

Although the instrument configurations and detectors at APS and BNL are similar, datasets collected of the same sample differ. These differences can be attributed to two effects: polymorph conversion and incident radiation. Since R05 is difficult to grow, the sample prepared at BNL was remeasured at APS. In the time between data collection, the metastable form R05 had begun to transform, introducing errors to the intensity of the measured reflections of the APS data. In contrast, the dataset collected at BNL is free from contamination by other phases. Nevertheless, because the operational wavelength employed at APS was longer (λ = 0.45336 Å), the pattern affords greater angular resolution. In order to come to the structure solution of R05, it was necessary to analyze both datasets.

The diffraction pattern collected at APS was indexed using the software program McMaille v3.04.[7] The 1D pattern was compared against cleaner datasets collected at NYU and BNL to ensure that only reflections related to R05 were included in the indexing file. By this process, the unit cell for R05 was determined as monoclinic with a = 11.479(4) Å, b = 11.030(1) Å, c = 10.840(6) Å, β = 118.23(1)°, V = 1209.3(44) Å^3.

2.3 Computational Crystal Structure Prediction

To obtain trial structures for crystal structure solution, we performed a systematic crystal structure prediction (CSP) based on evolutionary algorithms, as implemented in the USPEX code.[8–11] Only molecular geometry is used as input. The number of molecules per asymmetric unit (Z') and space group symmetries are user specified. Alternatively, the search can be constrained with an experimentally determined unit cell. GULP[12] and DFTB+[13] codes were used to perform the structure relaxations within USPEX. In our evolutionary search, the first generation of structures was created randomly in the given space groups. All structures were relaxed at ambient pressure and 0 K with enthalpy used as a measure of fitness. The energetically worst structures (40 %) were discarded and new generations were evolved by heredity and mutation operators as described elsewhere.[8] The best structure from each evolved generation was retained and runs were terminated after 50 generations.

Structural relaxations were performed in two steps. First, all structures were optimized by the GULP code[12] with the standard Dreiding force field[14] and partial charges assigned from the QEq method.[15] This was followed by further relaxation at the level of Density Functional Tight Binding with the DFTB+ code[13] and 3ob-3-1 parameter set.[16] In the final energy ranking stage, we chose the 100 lowest energy structures from the prediction. These were re-optimized with the optB88 functional[17] as implemented in VASP code[18] using the projector-augmented wave (PAW) method.[19] A plane wave kinetic energy cut-off of 1000 eV was used. For all geometry relaxation calculations, the

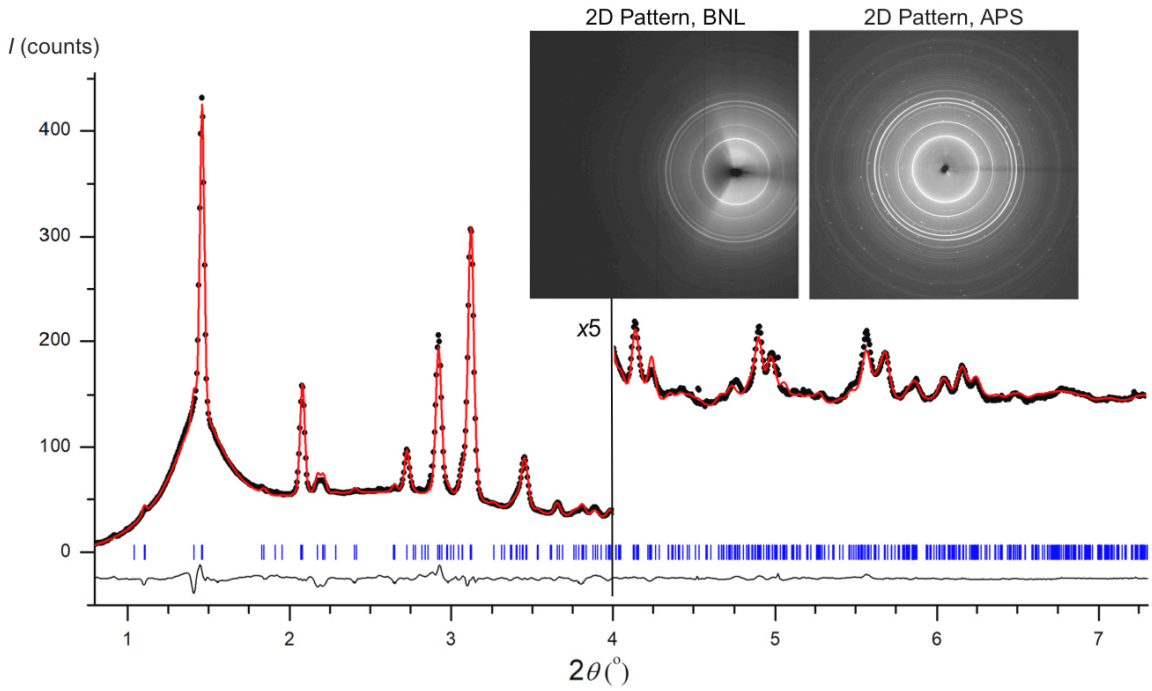

Fig. 2 Final Rietveld refinement of BNL synchrotron data (λ=0.18342 Å, 250 K) with 2D diffraction patterns collected at BNL and APS shown in the inset. Observed intensities are depicted as black circles while calculated intensities are illustrated as a red line. The difference curve is shown beneath in black. Blue ticks indicate positions of diffraction maxima.

Brillouin zone was sampled by uniform Γ-centered meshes with a reciprocal space resolution at least $2\pi \times 0.06$ Å, and convergence criteria of 1×10^{-5} eV/atom for total energies and 5×10^{-3} eV/ Å for forces.

A crystal structure search with $Z' = 1$ at ambient pressure was initially conducted for the 30 most common space groups. Although this successfully returned all known crystal structures of ROY deposited in the CSD (QAXMEH family), there were no reasonable solutions for R05. In our second attempt, the monoclinic cell obtained from experiment (a = 11.479 Å, b = 11.030 Å, c = 10.841 Å, β = 118.23°) was fixed and the query was constrained to search for structures with Z'=1 in $P2_1/c$, $C2$, and Cc, and Z' = 2 in $P2_1$ and Pc space groups. This identified the lowest energy structure as $P2_1$ with Z= 4, Z'= 2 and a simulated PXRD pattern in good agreement with the experimental data.

2.4 Structure Refinement

The synchrotron powder diffraction data collected at BNL was refined by the Rietveld method with TOPAS 4.2[20] ($C_{12}H_9N_3O_2S$, MW = 259.29 g/mol, ρ= 1.434 g/cm^3, λ= 0.18342 Å, T = 250 K). The geometry of each molecule was defined by a rigid body (RB). Rotation and translation parameters were simultaneously refined with the thiophene torsion angle θ_{thio} of each independent molecule in the asymmetric unit. This resulted in R_{wp} = 3.12% with $\theta_{thio,1}$ = 50.68°, and $\theta_{thio,2}$ = -31.94°.

The thermal displacement parameter (B_{eq}) was subsequently refined and bond length restraints were imposed for intermolecular interactions where the measured distance between contacts was less than the expected sum of vdW radii. Following this, all parameters were refined, including both the thiophene and phenyl ring torsion angles, resulting in an improvement to the overall molecular geometry. A refinement with all restraints removed (R_p = 2.17%, R_{wp} = 2.98%, R_{int} = 1.77%, GOF = 0.207) did not significantly alter the positions of non-hydrogen atoms; however, some bond lengths became too short. For this reason, bond length restraints were reintroduced and the structure was refined to a final R_p = 3.55%, R_{wp} = 3.00%, R_{int} = 1.78%, GOF = 0.208 with $\theta_{thio,1}$ = 44.9° and $\theta_{thio,2}$ = -34.0° and $\theta_{phen,1}$ = 11.5° and $\theta_{phen,2}$ = -19.2°. This structure was deposited to the CCDC (ref code 1822444). A comparison of the final refinement with the trial structure supplied by CSP closely agree. Periodic models of both structures expanded to 20-molecule clusters in COMPACK[21] resulted in a calculated highest root mean-square deviation of 0.189 Å.

3 Results and Discussion

3.1 Structure Analysis

All previously solved structures of ROY possess inversion symmetry and therefore contain heterochiral pairs of molecules in the unit cell. R05 is distinct from this group because it has two molecules in the asymmetric unit and lacks a center of symmetry. In the final Rietveld refinement, $\theta_{thio,1}$ = 44.9° and $\theta_{thio,2}$ = -34.9°; the molecules are twisted with opposite sense.

Color variations across different polymorphs of ROY are at-

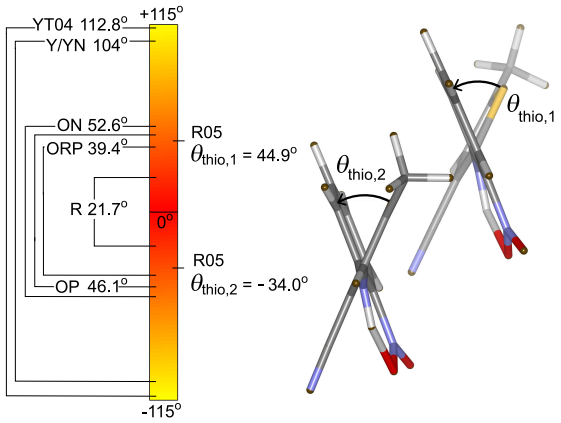

Fig. 3 The torsion angle defined by the S-C-N-C atom sequence (θ_{thio}) of all known ROY polymorphs compared to R05.

tributed to the conformational flexibility expressed by the torsion angle, θ_{thio} (Fig. 3).[2,22] In red form R, the aromatic rings are nearly co-planar ($\theta_{thio} = \pm 22°$, where the $\pm$ sign is due to inversion symmetry), leading to a greater degree of π conjugation, and a subsequent red shift in the visible absorption spectra.[22] In contrast, θ_{thio} is close to 90° in yellow forms Y, YT04, and YN (θ_{thio}=$\pm$(104-113)°). In forms OP, ON, and ORP, the torsion angle falls between these extremes ranging from $\pm$(39-53)°. Thus, as is outwardly suggested by its deep red-orange color, there is a kinship between R05 and the orange colored ROY polymorphs.

Like the previous seven structures solved, each molecule in R05 contains an intramolecular hydrogen bond between the amino and nitro groups. All known polymorphs of ROY, including R05, are characterized by a range of weak intermolecular interactions (Fig. 4). Among this group, intermolecular hydrogen bonds only exist in forms Y and Y04 between the cyano and amino group in neighboring molecules (C≡N···N-H).

Fingerprint plots derived from Hirshfeld surfaces were used to analyze packing in R05.[23–25] The Hirshfeld surface of a molecule in a crystal is constructed by partitioning space into regions where the electron distribution of a sum of spherical atoms for the molecule dominates the corresponding sum over the crystal. For each point on the surface, two distance properties are defined: d_e as the distance from a point to the nearest nucleus external to the surface, and d_i as the distance from a point to the nearest nucleus internal to the surface. 2D fingerprint plots are then derived from the Hirshfeld surface by plotting the fraction of points on the surface as a function of the pair (d_i, d_e). This concept has provided a convenient way to understand the intermolecular interactions and packing modes in molecular crystals.[25]

Table 1 Values of torsion angles in each ROY polymorph.

Polymorph	CSD entry	θ_{thio},°	θ_{phen},°
R	QAXMEH02	± 21.7	± 12.4
R05	this work	44.9/-34.0	11.8/-19.2
ORP	QAXMEH05	± 39.4	± 6.3
OP	QAXMEH03	± 46.1	± 12.4
ON	QAXMEH	± 52.6	± 6.4
YN	QAXMEH04	± 104.1	± 6.0
Y	QAXMEH01	± 104.7	± 4.4
YT04	QAXMEH12	± 112.8	± 10.4

A detailed Hirshfeld surface analysis of R, O, OP, ON, Y, YN, YT04 was made in 2007.[25] Here, we focus on the independent molecules in the asymmetric unit in R05 (R05-1 and R05-2), comparing each to forms R and Y. As shown in Fig. 5, the fingerprints of the two molecules in R05 are remarkably similar. Both contain a bright spot centered at d_i=1.8 Å, d_e=1.8 Å, which is characteristic of $\pi\cdots\pi$ stacking. In addition, the structures of R05-1 and R05-2 each feature "antennae" with internal (d_i) and external (d_e) distances of (1.3, 1.0) Å and (1.4, 1.0) Åthat are associated with CH···O and CH···O intermolecular distances that are shorter than the vdW distances. The antenna at (1.2, 1.2) Å corresponds to CH···H interactions. The similarities in both molecules suggests an almost identical local environment. This allows for the independent molecules to be treated as a pseduo-centrosymmetric pair. In contrast, R and Y exhibit quite different characteristics. In both R and Y, the center spot at (1.8, 1.8) Å is weaker and more diffuse, suggesting less uniform $\pi\cdots\pi$ stacking as compared to R05. In addition, the "antennae" of CH···N are notably stronger in Y, which agrees with the presence of C≡N···N-H intermolecular H bond.

The contributions of close intermolecular contacts shown in Fig. 6 provides another way to visualize packing differences in ROY forms R, Y, and R05. All structures are dominated by C···H, N···H, O···H, and H···H interactions. There are large changes in C···H and O···H across the series, while the changes in N···H and H···H are smaller. R05-1 and R05-2 again display very similar distributions, with only a slight difference in C···C, which can be assigned to $\pi\cdots\pi$ stacking. In contrast, Y has the smallest C···C contribution and largest extent of H···H. It does exhibit $\pi\cdots\pi$ stacking but the oblique angle of the molecules relative to each other in the crystal structure reduces the C···C interaction and results in greater C···C contributions than in the case of form R. Interestingly, the N···H contributions from Y are also smaller than in other polymorphs, although the "antennae" of CH···N, associated with the C≡N···N-H intermolecular H bond, have the longest spikes in Y (Fig. 5). This suggests that the total number of CH···N bonds is reduced but that they are stronger. On the other hand, R is quite different from both R05-1 and R05-2. Despite having a similar θ_{thio}, R has smaller C···C contributions but larger C···H. The C···C in R is from $\pi\cdots\pi$ between the benzene rings in chiral molecule pairs, while C···C in R05 is found between benzene-thiophene and thiophene-thiophene rings.

3.2 Energy Ranking

The rich polymorphism of ROY presents a challenge and an opportunity for computational chemists studying intermolecular interactions in organic crystals. The relative free energies of Y, YN YT04, R, OP, ON, and ORP were previously obtained by differential scanning calorimetry from melting and eutectic melting data.[2–4] The results indicate that the free energy of the seven ROY polymorphs characterized are separated by 1.5 kJ/mol at

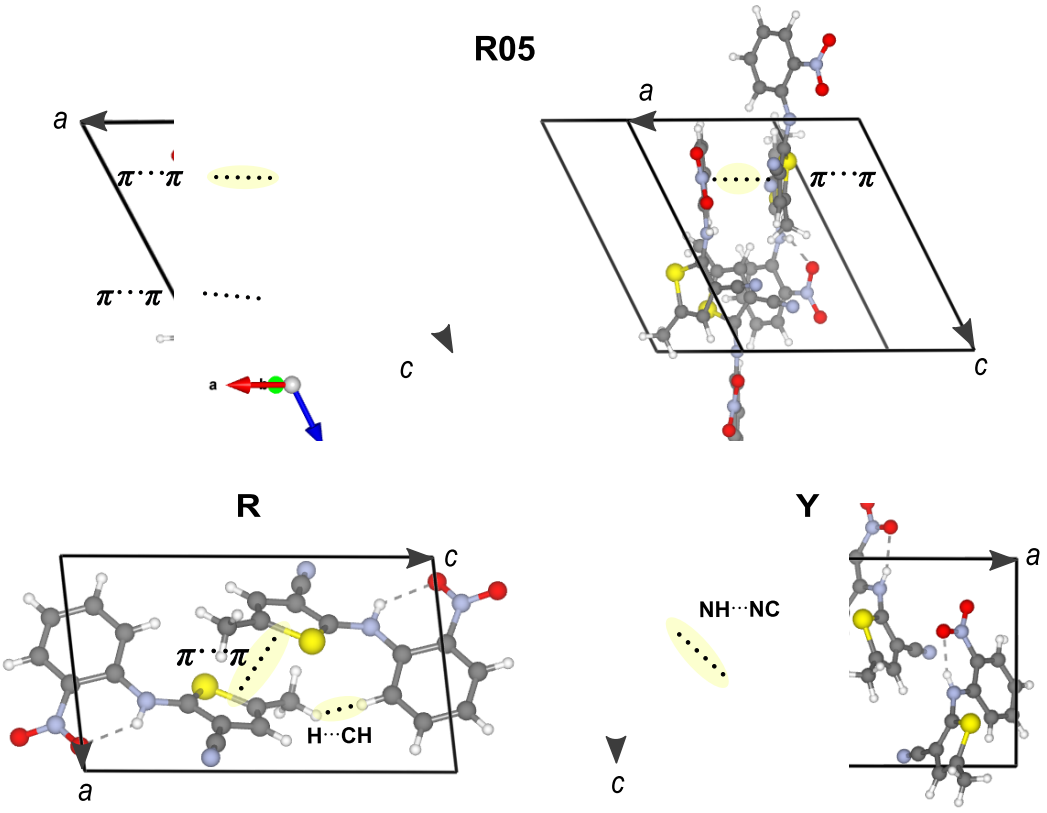

Fig. 4 Crystal structures for the selected ROY polymorphs (R, Y and R05) with some representative inter(intra)-molecular interactions highlighted.

40°C while the enthalpies span a range of 4 kJ/mol.[22] The stability of the polymorphs at 0 K was extrapolated from the enthalpy data as follows: Y (lowest) < YT04 < R < OP < ON < YN < ORP (highest).[22] There have been several subsequent studies that have sought to determine the energetic differences between ROY polymorphs through computational techniques, each employing varying levels of theory.[26–28] So far, computational predictions have differed from experimental results.

In 2005, Dunitz and Gavezotti[26] partitioned intermolecular energies into different contributions (Coulombic, polarization, dispersion and repulsions) between molecular pairs based on the molecular electron density distribution. The resulting ranking Y < YT04 < R < ON < OP < YN < ORP has nearly the same sequence as reported by Yu;[2] however, the energy difference (22 kJ/mol) is significantly larger than experimentally measured. Vasileiadis and co-workers[28] employed a similar semi-empirical approach based on distributed multipole analysis and found YN < Y < R < YT04 < OP < ORP < ON, with a range of 10.2 kJ/mol between YN and ON.

The first DFT study on ROY polymorphs[27] sorted the stability of the forms as ORP < ON < Y < R < OP < YN < YT04 at 0 K. Here, the energy separation between YT04 and ORP was determined to be 20 kJ/mol. This wide range in values indicated that lattice energy alone is insufficient to determine energy rankings. Subsequent calculations were performed that incorporated the effect of the crystallization force, accounting for local changes to the electronic structure as result of packing.[27] In this updated model, the ranking sequence of ROY polymorphs was determined as Y < R < ON < ORP < YN < YT04 < OP with an energy difference of 10.1 kJ/mol.

New developments in computational methodologies have improved energy rankings, describing vdW interactions in the framework of DFT.[17] Accuracy within 5 kJ/mol has been achieved with vdW-inclusive DFT.[29] Even greater accuracy (within 1 kJ/mol) can be obtained by using computationally demanding wave-function based electronic structure methods.[30] Moreover, in the most recent blind test organized by Cambridge Crystallographic Data Center (CCDC), substantial improvements were made in the use of hierarchical approaches to ranking structures and in the application of density-functional approximations.[31] These advances, together with the new structure solution of R05, encouraged us to perform an updated benchmark of energy rankings for ROY polymorphs at the DFT level.[27]

We selected 40 low-energy structures after merging results from all CSP runs, and studied the lattice energy versus density relation at the level of optPBE using the VASP code (see Fig. 7a). Clearly, all of the observed polymorphs cover a range of ≈6 kJ/mol, which is significantly smaller than the previous studies based on semi-empirical approaches.[26,28] Nevertheless, there do exist a number of hypothetical structures with close stabilities relative to the experimental structures. It is unclear whether they are real structures which have not been found by experiment, or they

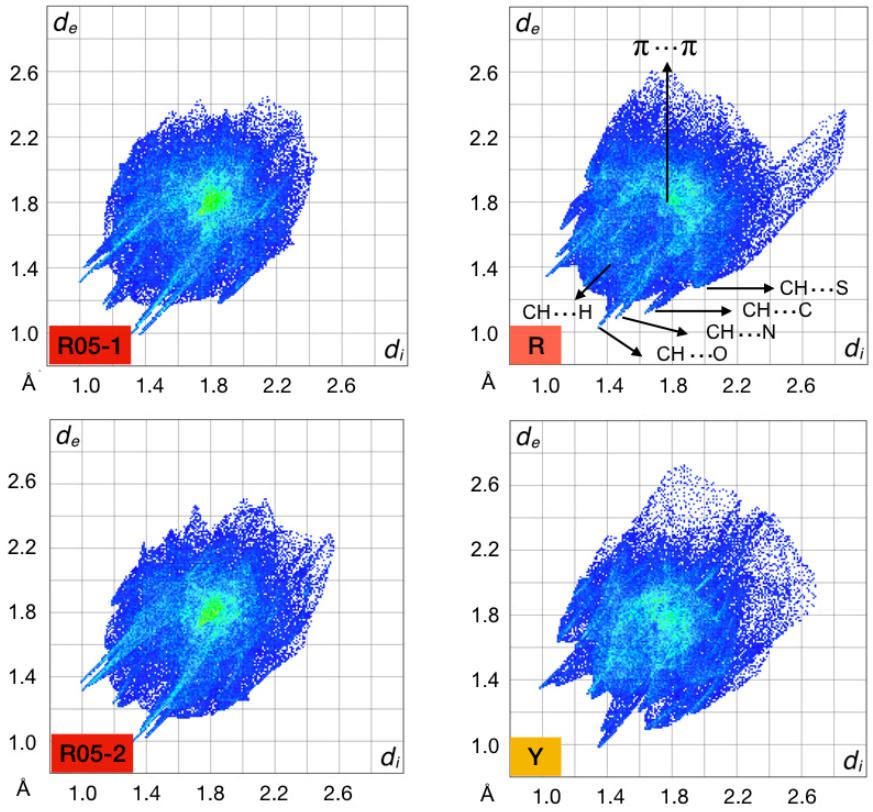

Fig. 5 2D Hirshfeld fingerprint plots for the selected ROY polymorphs (R, Y, R05-1 and R05-2). The representative intermolecular interactions are also highlighted in the plots.

were misranked by optPBE functional. Moreover, the stability ranking predicted by our calculations strongly deviates from experimental data.[3] Form Y, the polymorph previously determined as most stable at ambient conditions,[3] had the highest enthalpy at 0 K among all ROY forms in our calculations. We were not surprised. In a recent study on the polymorphs of coumarin, we discovered that different vdW-inclusive models yielded inconsistent rankings.[32] Thus, we performed another benchmark test on ROY with other vdW-inclusive models, namely PBE-D3[33] in VASP, and PBE+MBD and PBE0+MBD[34] in FHI-aims.[35] Although the ranking varies according to the choice of computational model, all calculations exhibit the same general trend (Fig. 7b). That is, red colored forms are most stable, followed by orange. Yellow forms are least stable in terms of enthalpy. This overall ranking is contrary to experimental data and to previous computational studies which have either ranked Y or YT04 as the most stable form. From a structural perspective, Y and YT04 differ from other forms due to the presence of weak intermolecular hydrogen bonds (C≡N···N-H). This subtlety does not seem to be recognized in our DFT models. Disagreement between our calculations and previous work in DFT on ROY[27] may also stem from the choice of functional basis set and dispersion correction models. Despite this, the energy range determined in the current study is significantly smaller as compared to that found previously,[27] suggesting an overall improvement of DFT-vdW inclusive methodology. Furthermore, we emphasize that our DFT calculations were performed at 0 K and ignore entropic contributions, while the previous stability ranking relied upon the free energy difference derived from the experimental eutectic melting data.[3] Thus, the deviation between experiment and theory might be due to a temperature effect. Calculated entropic contributions are typically small but nevertheless sufficient to switch the energy ranking for different polymorphs.[36] Indeed, our recent work on coumarin indicates that both harmonic and anharmonic vibrations might make non-negligible contributions to the total free energy. An investigation on possible origins for the discrepancy between theory and experiment remains the subject of future work.

3.3 Twisting

It is hard to make R05 from the melt. No doubt this is the reason why it was the last polymorph of ROY to have been discovered. During the process of melting and recrystallizing samples, we observed features of YN that had not been previously described in the literature. At high magnification, this form displays the tell-tale sign of twisting – optical banding. Helicoidal twisting of lamellae in molecular crystals is actually an extraordinarily common phenomenon for crystals grown under high driving force.[37] It has been said that 25% of simple molecular crystals are twisted.[38] This is a credible estimate. Thus, since seven of ten ROY polymorphs can be grown from the melt, it would be

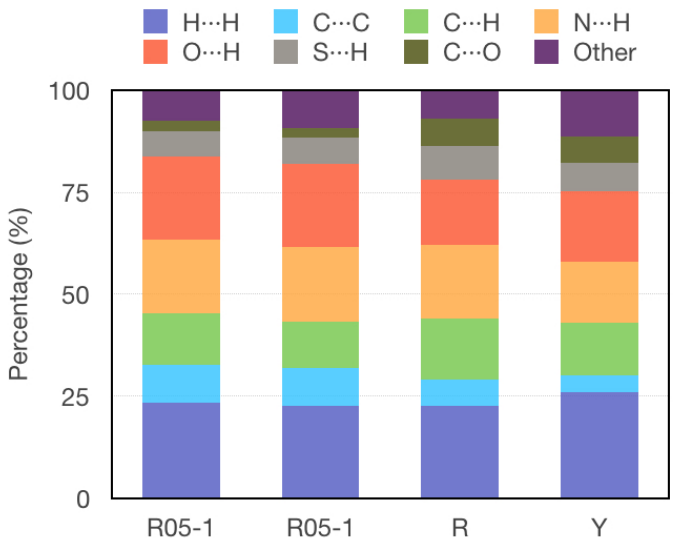

Fig. 6 Percent contributions of various intermolecular interactions to Hirshfeld area in R05-1, R05-2, R, and Y.

improbable for ROY to be twist free.

The optical properties of YN were measured with a Mueller matrix microscope that employs dual continuously rotating retarders, installed before and after the sample plane, to modulate the polarization state of light. The operational theory of our system is similar to earlier instrument designs.[39–41] In short, the continuous rotation of each retarder creates a smoothly varying time-dependent intensity signal at the detector that can be analyzed to recover the 16 elements of the 4x4 Mueller matrix, **M**. Here, **M** is a polarization transfer matrix that describes how a sample transforms a four-element input polarization state vector ($\mathbf{S}_{in}$) to its output ($\mathbf{S}_{out}$). If **M** is nondepolarizing, the 16 elements of the Mueller matrix simplify to seven.[42] These seven parameters form a 4x4 matrix **L**. **M** is related to **L** by the matrix exponential,[39] $\mathbf{M} = \exp \mathbf{L}$ where

$$\mathbf{L} = \begin{bmatrix} -A & -LD & -LD' & CD \\ -LD & -A & CB & LB' \\ -LD' & -CB & -A & -LB \\ CD & -LB' & LB & -A \end{bmatrix}$$

The parameters LD, LB, CD, and CB refer to linear dichroism, linear birefringence, circular dichroism, and circular birefringence, respectively. Strictly speaking, the matrix **L** only holds for normal incidence measurements of homogenous media with plane parallel surfaces.[43] Helicoidally twisted spherulites do not fit this definition. Nevertheless, the parameters in **L** provide a convenient basis to understand the optical properties of the aggregate.[43]

Measurements were performed at normal incidence over a range of wavelengths. A precession correction algorithm was applied to the images in order to remove beam steering artifacts caused by imperfect optics.[44] Minimal depolarization allowed for **M** to be reduced to **L**. Fig. 8 plots the magnitude of linear birefringence ($|LB|$) of a so-called banded spherulite of YN measured at 620 nm (20x). The concentric light and dark bands indicate in-phase helicoidal precession of radially aligned fibers. The spacing between dark bands is equal to half the pitch.

Thus, R05 is chiral because of its crystal structure whereas YN is chiral because of its morphology. Although the coexistence of new polymorphs from the melt with twisted morphologies is commonplace, a chiral space group is not a prerequisite to a twisted form; YN crystallizes in the centric space group $P\bar{1}$ but nevertheless exhibits twisting. In contrast, the crystal structure of R05 is chiral but spherulites grown from the melt under the same conditions as YN do not twist.

4 Conclusions

Pairing high-resolution X-ray powder diffraction with crystal structure prediction techniques is an effective method for determining the structures of metastable polymorphs.[10,32,45] Indeed, DFT optimization of candidate structures during the process of crystal structure solution allows for chemically sensible structure models to be determined even when the quality of diffraction data is modest. In this manuscript, we employed such a multipronged approach to yield the structure of R05, the most recently discovered polymorph of ROY. R05 is acentric with two independent molecules that have opposite twists. Nevertheless, according to Hirshfeld analysis, the independent molecules have comparable local environments. Although CSP was applied with success to the problem of crystal structure solution, our DFT based vdW-inclusive calculations still do not converge to the experimentally determined energy rankings, indicating that ROY polymorphism remains a challenge for computational chemistry.

5 Acknowledgements

This work was supported partially by the MRSEC Program of the National Science Foundation under Award Number DMR-1420073. B.K. is grateful for support from the U.S. National Science Foundation (DMR-1608374) and the National Institutes of Health (5R21GM107774-02). Q.Z. is grateful for support from the National Nuclear Security Administration under the Stewardship Science Academic Alliances program through DOE Cooperative Agreement DE-NA0001982. Calculations were performed at computing resources from XSEDE and Center for Functional Nanomaterials (under contract no. DE-AC02-98CH10086). This research used synchrotron X-ray resources of the Advanced Photon Source and the National Synchrotron Light Source II, U.S. Department of Energy (DOE) Office of Science User Facilities operated for the DOE Office of Science by Argonne National Laboratory and Brookhaven National Laboratory, respectively, under Contract No. DE-AC02-06CH11357 and DE-SC0012704. Q.Z. thanks Alexandre Tkatchenko and Johannes Hoja for help in MBD calculation in the FHI-aims code.

6 Conflict of interest

The authors declare no conflict of interest.

References

1 G. Stephenson, T. Borchardt, S. Byrn, J. Boyer, S. Snorek, C. Bunnell and L. Yu, *J. Pharm. Sci.*, 1995, **84**, 1385–1386.

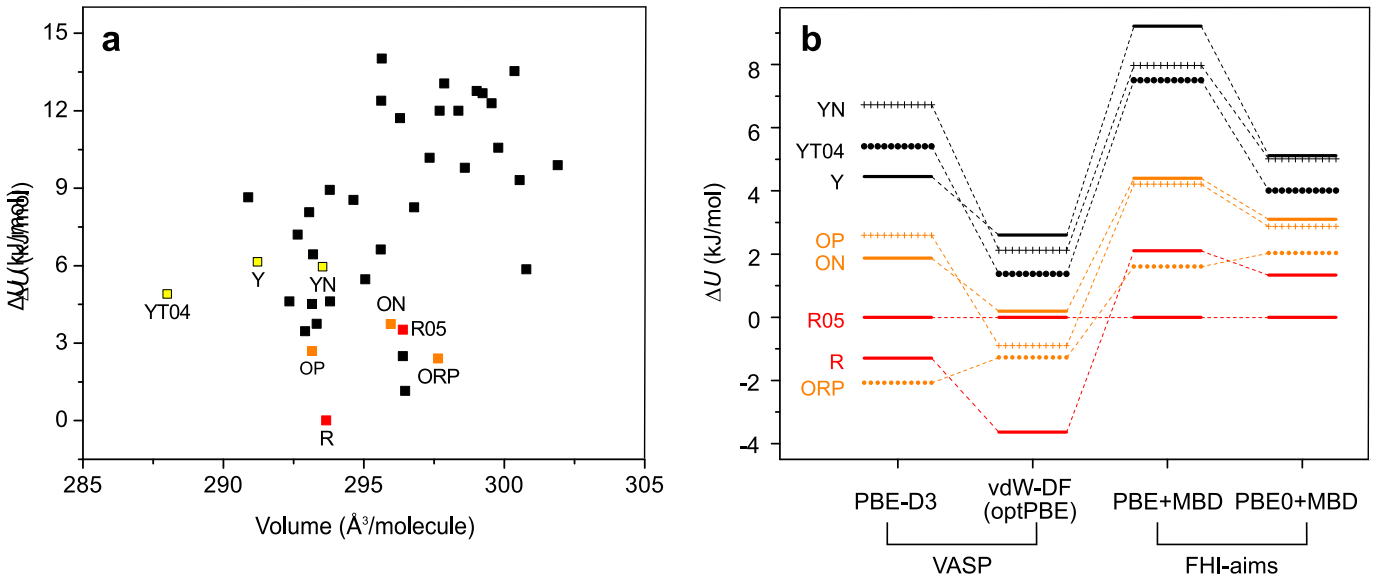

Fig. 7 (a) Lattice energy versus molecular volume at the optPBE level. (b) Energy rankings for the eight known polymorphs of ROY with different vdW-inclusive models.

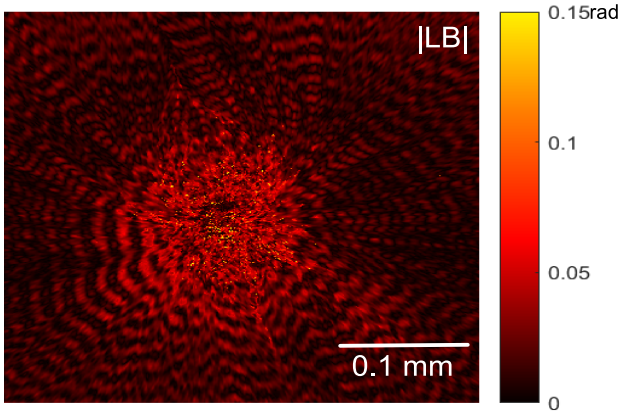

Fig. 8 The oscillation in the magnitude of the linear birefringence (|LB|) of a banded spherulite of YN measured at 620 nm is indicative of twisting.

2 L. Yu, G. A. Stephenson, C. A. Mitchell, C. A. Bunnell, S. V. Snorek, J. J. Bowyer, T. B. Borchardt, J. G. Stowell and S. R. Byrn, *J. Am. Chem. Soc.*, 2000, **122**, 585–591.

3 S. Chen, H. Xi and L. Yu, *J. Am. Chem. Soc.*, 2005, **127**, 17439–17444.

4 S. Chen, I. Guzei and L. Yu, *J. Am. Chem. Soc.*, 2005, **127**, 9881–9885.

5 V. Lopez-Mejias, J. W. Kampf and A. J. Matzger, *J. Am. Chem. Soc.*, 2012, **134**, 9872–9875.

6 S. P. Delaney, D. Pan, S. X. Yin, T. M. Smith and T. M. Korter, *Cryst. Growth Des.*, 2013, **13**, 2943–2952.

7 A. Le Bail, *Powder Diffraction*, 2004, **19**, 249–254.

8 Q. Zhu, A. R. Oganov, C. W. Glass and H. T. Stokes, *Acta Crystallogr. Sect. B*, 2012, **68**, 215–226.

9 A. O. Lyakhov, A. R. Oganov, H. T. Stokes and Q. Zhu, *Comput. Phys. Comm.*, 2013, **184**, 1172 – 1182.

10 Q. Zhu, A. G. Shtukenberg, D. J. Carter, T.-Q. Yu, J. Yang, M. Chen, P. Raiteri, A. R. Oganov, B. Pokroy, I. Polishchuk, P. J. Bygrave, G. M. Day, A. L. Rohl, M. E. Tuckerman and B. Kahr, *J. Am. Chem. Soc.*, 2016, **138**, 4881–4889.

11 J. Yang, C. T. Hu, X. Zhu, Q. Zhu, M. D. Ward and B. Kahr, *Angew. Chem. Int. Ed.*, 2017, **56**, 10165–10169.

12 J. D. Gale and A. L. Rohl, *Molecular Simulation*, 2003, **29**, 291–341.

13 B. Aradi, B. Hourahine and T. Frauenheim, *J. Phys. Chem. A*, 2007, **111**, 5678–5684.

14 S. L. Mayo, B. D. Olafson and W. A. Goddard, *J. Phys. Chem.*, 1990, **94**, 8897–8909.

15 A. K. Rappe and W. A. Goddard III, *J. Phys. Chem.*, 1991, **95**, 3358–3363.

16 M. Gaus, A. Goez and M. Elstner, *J. Chem. Theory Comp.*, 2012, **9**, 338–354.

17 J. Klimeš and A. Michaelides, *J. Chem. Phys.*, 2012, **137**, 120901.

18 G. Kresse and J. Furthmüller, *Phys. Rev. B*, 1996, **54**, 11169–11186.

19 P. E. Blöchl, *Phys. Rev. B*, 1994, **50**, 17953.

20 *Bruker AXS TOPAS v4: General profile and structure analysis software for powder diffraction data. User's Manual*, Bruker

AXS, Karlsruhe Germany, 2008.
21 J. A. Chisholm and S. Motherwell, *J. Appl. Crystallogra.*, 2005, **38**, 228–231.
22 L. Yu, *Acc. Chem. Res.*, 2010, **43**, 1257–1266.
23 F. L. Hirshfeld, *Theor. Chem. Acc.*, 1977, **44**, 129–138.
24 M. A. Spackman and J. J. McKinnon, *CrystEngComm*, 2002, **4**, 378–392.
25 J. J. McKinnon, F. P. Fabbiani and M. A. Spackman, *Cryst. Growth Des.*, 2007, **7**, 755–769.
26 J. Dunitz and A. Gavezzotti, *Cryst. Growth Des.*, 2005, **5**, 2180–2189.
27 T. Li, P. W. Ayers, S. Liu, M. J. Swadley and C. Aubrey-Medendorp, *Chem. Eur. J.*, 2009, **15**, 361–371.
28 M. Vasileiadis, A. V. Kazantsev, P. G. Karamertzanis, C. S. Adjiman and C. C. Pantelides, *Acta Crystallogr. Sect. B*, 2012, **68**, 677–685.
29 G. J. Beran, *Chem. Rev.*, 2016, **116**, 5567–5613.
30 J. Yang, W. Hu, D. Usvyat, D. Matthews, M. Schütz and G. K.-L. Chan, *Science*, 2014, **345**, 640–643.
31 A. M. Reilly, R. I. Cooper, C. S. Adjiman, S. Bhattacharya, A. D. Boese, J. G. Brandenburg, P. J. Bygrave, R. Bylsma, J. E. Campbell, R. Car *et al.*, *Acta Crystallogr. Sect. B*, 2016, **72**, 439–459.
32 A. G. Shtukenberg, Q. Zhu, D. J. Carter, L. Vogt, J. Hoja, E. Schneider, H. Song, B. Pokroy, I. Polishchuk, A. Tkatchenko, A. R. Oganov, A. L. Rohl, M. E. Tuckerman and B. Kahr, *Chem. Sci.*, 2017, **8**, 4926–4940.
33 S. Grimme, J. Antony, S. Ehrlich and H. Krieg, *J. Chem. Phys.*, 2010, **132**, 154104.
34 A. Tkatchenko, R. A. DiStasio Jr, R. Car and M. Scheffler, *Phys. Rev. Lett.*, 2012, **108**, 236402.
35 V. Blum, R. Gehrke, F. Hanke, P. Havu, V. Havu, X. Ren, K. Reuter and M. Scheffler, *Comput. Phys. Commun.*, 2009, **180**, 2175–2196.
36 J. Nyman and G. M. Day, *CrystEngComm*, 2015, **17**, 5154–5165.
37 A. Shtukenberg, Y. Punin, A. Gujral and B. Kahr, *Angew. Chem. Int. Ed.*, 2014, **53**, 672–699.
38 F. Bernauer, *"Gedrillte" Kristalle*, Gebrüder Borntraeger, 1929.
39 R. M. A. Azzam, *Opt. Lett.*, 1978, **2**, 148–150.
40 C. Chen, I. An, G. Ferreira, N. Podraza, J. Zapien and R. Collins, *Thin Solid Films*, 2004, **455-456**, 14 – 23.
41 O. Arteaga, M. Baldrís, J. Antó, A. Canillas, E. Pascual and E. Bertran, *Appl. Opt.*, 2014, **53**, 2236–2245.
42 S. Cloude, *Polarisation: Applications in Remote Sensing*, Oxford Univ. Press, 2010.
43 X. Cui, S. M. Nichols, O. Arteaga, J. Freudenthal, F. Paula, A. G. Shtukenberg and B. Kahr, *J. Am. Chem. Soc.*, 2016, **138**, 12211–12218.
44 S. M. Nichols, *PhD thesis*, New York University, 2018.
45 A. G. Shtukenberg, C. T. Hu, Q. Zhu, M. U. Schmidt, W. Xu, M. Tan and B. Kahr, *Cryst. Growth Des.*, 2017, **17**, 3562–3566.